



Degradation of ciprofloxacin by 280 nm ultraviolet-activated persulfate: Degradation pathway and intermediate impact on proteome of *Escherichia coli*

Jin-shao Ye ^{a, b}, Juan Liu ^a, Hua-se Ou ^{a,*}, Lin-lin Wang ^{a, b}

^a School of Environment, Guangzhou Key Laboratory of Environmental Exposure and Health, Guangdong Key Laboratory of Environmental Pollution and Health, Jinan University, Guangzhou 510632, China

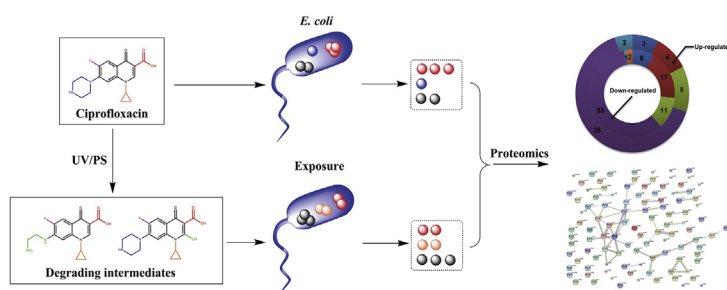
^b Joint Genome Institute, Lawrence Berkeley National Laboratory, Walnut Creek 94598, CA, USA



HIGHLIGHTS

- 280 nm ultraviolet/persulfate induces moderate transformations of ciprofloxacin.
- The transformations involve breakages of piperazine ring and quinolone backbone.
- The incomplete transformations reduce the antibacterial activity of ciprofloxacin.
- The response of *E. coli* protein network is evaluated by iTRAQ-based proteomic.
- Degraded CIP induces less stress on the metabolic process than intact CIP.

GRAPHICAL ABSTRACT



ARTICLE INFO

Article history:

Received 8 July 2016

Received in revised form

8 September 2016

Accepted 8 September 2016

Available online 30 September 2016

Handling Editor: Shane Snyder

Keywords:

Ultraviolet activated persulfate

Antibiotics

Advanced oxidation process

Proteomics

Toxicological assessment

Water treatment

ABSTRACT

In this study, the degradation of ciprofloxacin (CIP) was explored using ultraviolet activated persulfate (UV/PS) with 280 nm ultraviolet light-emitting diodes (UV-LEDs), and the toxicological assessment of degrading intermediates was performed using iTRAQ labeling quantitative proteomic technology. The quantitative mass spectrum results showed that 280 nm UV/PS treatment had a high transformation efficiency of CIP ($[CIP] = 3 \mu\text{M}$, $[S_2O_8^{2-}] = 210 \mu\text{M}$, apparent rate constants 0.2413 min^{-1}). The high resolution mass spectrum analyses demonstrated that the primary intermediates included $C_{15}H_{16}FN_3O_3$ (m/z 306.1248) and $C_{17}H_{18}FN_3O_4$ (m/z 348.1354). The former one was formed by the cleavage of piperazine ring, while the later one was generated by the addition of a hydroxyl on the quinolone backbone. The toxicological assessment demonstrated that 56 and 110 proteins had significant up regulations and down regulations, respectively, in the *Escherichia coli* exposed to degraded CIP compared to untreated CIP. The majority of up-regulated proteins, such as GapA, SodC, were associated with primary metabolic process rather than responses to stress and toxic substance, inferring that the moderate UV/PS treatment can reduce the antibacterial activity of CIP by incomplete mineralization. Consequently, these results provided a novel insight into the application of UV-LED/PS treatment as a promising removal methodology for quinolones.

© 2016 Elsevier Ltd. All rights reserved.

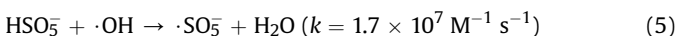
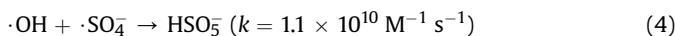
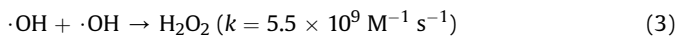
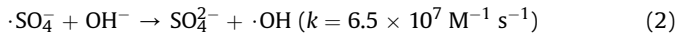
* Corresponding author.

E-mail address: [\(H.-s. Ou\)](mailto:touhause@jnu.edu.cn)

1. Introduction

Quinolones are used as common antibiotics for the treatments of human and animal diseases worldwide. Unfortunately, the robustness of quinolones against conventional microorganism-based wastewater treatment plants resulted in their undesired discharge into natural water bodies (Lapara et al., 2011; Qinjin et al., 2014). Recently, numerous researchers have found that quinolones in the environment aggravated several ecological problems, such as the increase of antibiotic resistance in bacteria (Oberlé et al., 2012), the physiological teratogenesis of plants/algae (Ludmilla et al., 2010) and the chronic genotoxicity/carcinogenic potential to organisms (Min et al., 2014). It was reported that the removal of quinolones in wastewater treatment plants was mainly due to their sorption onto activated sludge but not biodegradation process (Zhou et al., 2013). Therefore, worldwide researchers attempt to develop cost-effective non-biological treatment methods for quinolones.

Various advanced oxidation processes (AOPs), such as ozonation (Liu et al., 2012), Fenton oxidation (Pi et al., 2014a), TiO₂ photocatalysis (Doorslaer et al., 2013) and ultraviolet/H₂O₂ (UV/H₂O₂) process (Ou et al., 2016), were proved to be effective. Recently, activated persulfate (PS, S₂O₈²⁻) oxidation is considered as an alternative AOP due to its simple operation, high oxidizability and wide application. Heating, UV illumination and ferrous ion all can activate PS to generate sulfate radical (SO₄^{·-}, E⁰ = 2.65–3.10 V) (Avetta et al., 2014). Once the SO₄^{·-} is generated, it can induce a chain of reactions involving the formation of other active species (Eqs. (1)–(5)).



Besides SO₄^{·-}, hydroxyl radical (OH[·]) was confirmed to be responsible for the degradation of quinolones in heating-PS system (Ji et al., 2014), but it was reported that UV-A (365 nm) activated SO₄^{·-} had a low reaction rate with quinolones (An et al., 2010). Since quinolones have a significant absorption at ~275 nm UV-C (Ou et al., 2016), UV-C/PS may induce a multiple degradation, including photolysis and radical oxidation, of quinolone, which can be more efficient than heating, ferrous ion or UV-A activated PS. It was reported that the 254 nm UV/PS had a higher efficiency than UV/H₂O₂ for quinolones removal in distilled water or wastewater (Mahdi-Ahmed and Chiron, 2014). However, the further identification of degrading intermediates and the safety of UV-C/PS degrading quinolones are still unknown.

In actual water treatment, full mineralization of antibiotics will likely be infeasible due to the competitive reactions of various other contaminants (Dodd et al., 2009). Furthermore, the operational cost also limits the degradation level of targeted antibiotics. Therefore, a moderate degradation may be feasible. The degrading intermediate determination and relevant toxicological evaluation can be used to support this application prospecton. To this end, a series of traditional toxicological evaluation techniques, such as antibacterial activity assay, were applied to investigate the toxicity of degrading intermediates at cellular level (Paul et al., 2010; Rodrigues-Silva et al., 2013). However, these studies provided limited information regarding to the negative impacts of intermediates on molecular

and metabolic functions. Furthermore, whether the generated products have specific toxic activities against human and other species in environment is also needed to be evaluated (Brienza et al., 2016). The action mechanism of quinolones involves a series of interactions with specific functional proteins and metabolic pathways, thus, the safety assessment of their degrading reactions required a global investigation in the perspective of protein network level.

Within the last decade, the development of isobaric tags for relative and absolute quantitation (iTRAQ) labeling quantitative proteomic technology provides us with a novel and powerful technique that can identify, characterize, and quantify protein expression in cells, tissues or organisms under given conditions. Several researches already focused on applying quantitative proteomic to screen useful genes and proteins for specific chemical compound degradation in functional microbes (Kjeldal et al., 2015), or to perform the toxicology and risk assessment of environmental contaminants (Liu et al., 2016). However, there is no study which uses iTRAQ proteomic for the safety evaluation of a water treatment method. The potential findings in regard to the safety of degrading intermediates on protein network level can provide guidance for the regulation of reaction extent from complete mineralization to a moderate degradation, which may reduce the energy and chemical consumption.

In our previous study, the 280 nm irradiation was proved to have the highest degrading efficiency of ciprofloxacin (CIP) among 255–365 nm ultraviolet light-emitting diodes (UV-LEDs) (Ou et al., 2016). Therefore, the 280 nm UV-LED was deliberately used to activate PS in this research. The degradation effectiveness and intermediates were determined using high resolution mass spectrum (HRMS), and the iTRAQ proteomics analysis was used to evaluate the impact of CIP and its degrading intermediates on *Escherichia coli*. This study was expected: (1) to describe the degradation pattern of CIP in the 280 nm UV/PS system, (2) to explore the potential application of iTRAQ proteomics for the safety evaluation of AOPs, and (3) to prove the feasibility of applying moderate degradation for quinolone elimination.

2. Methods

2.1. Chemical reagents

All chemical reagents in the study were of the highest purity available (Text S1).

2.2. UV-LED micro-module and degradation experiments

A UV-LED irradiation micro-module was designed and assembled. The detailed structure and constitution of this device were described in our previous study (Ou et al., 2016). The irradiating intensity of the UV-LEDs were measured using a HAAS-3000 light spectrum irradiation meter (Everfine, China). The average irradiation intensity of the 280 nm UV-LED chips was 0.023 mW cm⁻² at the surface of the reaction solution. The irradiation dose was calculated as:

$$\text{Dose} = \text{Int} \times T \quad (6)$$

where Int is the irradiation intensity and T stands for the irradiation time (s), and the irradiation dose has a unit of mJ cm⁻².

Twenty milliliters of CIP solution at 1 mg L⁻¹ (3 μM) was spiked into the quartz vessel. In the UV/PS experiments, the initial concentration of Na₂S₂O₈ was in the range of 10–200 mg L⁻¹ (42–840 μM). The solution was maintained at 25 ± 2 °C, pH = 6.8–7.2, and its uniformity was achieved by shaking the

vessel at 60 r min^{-1} . The reaction was initiated by turning on the UV-LED array. At a pre-defined time, ascorbic acid, at a concentration that was stoichiometrically equivalent to the initial $\text{Na}_2\text{S}_2\text{O}_8$ dose, was added to stop the reaction. Afterwards, 20 mL of the sample was transferred into a brown amber tube and then stored at 4°C before sample analysis. The UV-only and PS-only control experiments were included in the experimental design. In the influence factors experiments, the solution pH was adjusted using a 5.0 mM phosphate-buffered solution, and predetermined amount of NaCl , NaHCO_3 , Na_2SO_4 or humic acid was added into the solution.

2.3. Ion chromatography and total organic carbon (TOC) analyses

The determination of F^- and NO_3^- was performed using an ICS-2500 analyzer (Dionex, USA) with an ED50A detector. A DIONEX IonPac® AS15 column was used with 30.0 mM NaOH solution as the mobile phase. Furthermore, the TOC was measured using a Liquid TOC trace analyzer (Elementar, Germany).

2.4. Qualitative and quantitative analysis of CIP and its intermediates

The identification of intermediates was performed using a TripleTOF 5600+ HRMS (Applied Biosystems SCIEX, USA). The quantitative analysis of CIP and degrading intermediates was performed using a TripleQuad 5500 tandem mass spectrometer (Applied Biosystems SCIEX, USA). The detailed operational procedure and parameters are presented in [Text S2](#).

2.5. Proteomics analysis preparation

In the proteomics analysis, *E. coli* ATCC11303 was used as the model microorganism, which was inoculated into 100 mL culture medium at 100 r min^{-1} for 12 h. Subsequently, the cells were separated from the medium by centrifugation at 3500g for 10 min and were washed three times. The cells at 0.1 g L^{-1} were inoculated into 20 mL medium containing (mg L^{-1}) 30 KH_2PO_4 , 70 NaCl , 30 NH_4Cl , 10 MgSO_4 , 30 beef extract, 100 peptone and 1 CIP or its intermediates in the dark at 25°C on a rotary shaker at 100 r min^{-1} for 24 h. After exposure, the cells were separated and washed using phosphate buffer solution for protein extraction. The further protein extraction procedure is presented in [Text S3](#).

2.6. Protein digestion, iTRAQ labeling and analysis

Briefly, proteins from each sample were reduced with 10 mM dithiothreitol for 1 h at 37°C . The cysteines were blocked with 1 μl blocking reagent for 10 min at room temperature. The protein samples were added in 10 KD Amicon Ultra-0.5 centrifugal filter devices, followed by centrifugation at $12,000 \text{ r min}^{-1}$ for 20 min. After removal of the liquid, the samples in filter devices were digested by 50 μl trypsin at 4% w/w overnight at 37°C . Subsequently, the samples were centrifuged, and 1 μg trypsin was added to each filter for 2 h. After centrifugation, liquid in the collection tube was collected.

The tryptic peptides were labeled with iTRAQ reagent multiplex kit according to the manufacturer's instructions. Subsequently, the labeled peptides were dried in a vacuum concentrator. The samples were then resolved with solution containing 2% v/v CAN and 0.1% v/v formicacid, centrifuged at 12,000 r/min for 20 min, and detected by a TripleTOF 5600+ HRMS (Applied Biosystems SCIEX, USA) equipped with a Nanospray III source and a NanoLC 400 system. All HRMS data were combined to search the NCBI database (<http://www.ncbi.nlm>). To avoid false positives, the identified proteins were subjected to an in-house BLAST search at NCBI to confirm the

matches. The detailed information of further protein identification is presented in [Text S4](#).

2.7. Inhibition halo experiment

The inhibition halo experiment was performed to evaluate the reduction of antibacterial activity. The agar plates were inoculated with $1.2 \times 10^8 \text{ CFU mL}^{-1}$ *E. coli*, and parallel 10- μL treated samples were separately spiked on agar plates. The plates were then cultured at 37°C for 24 h, and the inhibition halo diameter was measured.

3. Results and discussion

3.1. Degradation kinetics

The degradation efficiencies in the UV-only, PS-only and UV/PS experiments are presented in [Fig. 1a](#). A slight variation in the CIP concentration was observed in the PS-only experiment, indicating that inactivated PS had a negligible effect on CIP. To the contrary, illumination at 280 nm UV resulted in a significant decrease of CIP. For 3 μM (1 mg L^{-1}) CIP, the removal effectiveness reached ~70% after 60 min irradiation. Furthermore, the treatment using 280 nm UV/PS was more effective than UV-only treatment, and its removal efficiency reached ~97% within 20 min. Based on the fitting calculation, the degradation of CIP by 280 nm UV/PS was confirmed to be a pseudo-first order reaction. The related kinetics curves are presented in [Fig. 1b](#). The apparent rate constant of UV-only treatment was 0.0247 min^{-1} , and the half-life of CIP was 28.1 min ([Table S1](#)). Compared with the results of the UV-only experiments, the apparent rate constant in the UV/PS system increased to 0.2442 min^{-1} with a half-life of 2.8 min, which may be ascribed to the promotion of $\text{SO}_4^{\cdot-}$ oxidation. The degradation efficiencies and kinetics in the experiments involving different influence factors are presented in [Text S4](#).

The variation of TOC is presented in [Fig. 1c](#). For a 3 μM CIP solution, the TOC was $0.593 \pm 0.061 \text{ mg L}^{-1}$ at the initial time. After a reaction time of 60 min, only a slight variation of TOC was observed in the 280 nm UV/PS system. This low mineralization efficiency indicated that UV/PS oxidation induced an incomplete transformation of CIP. Since CIP contained one fluorine atom and several nitrogen atoms ([Fig. S2](#)), the formation of inorganic anions, such as F^- and NO_3^- , can also describe its transformation pattern in the UV/PS system. The variations of F^- and NO_3^- are shown in [Fig. 1d](#). The dosage of F^- increased from 0 to 0.027 mg L^{-1} , suggesting a fracture of C–F bond in CIP. Theoretically, 3 μM CIP contained 0.057 mg L^{-1} fluorine, which was higher than the observed F^- dosage. Furthermore, only a slight increase of NO_3^- was observed, implying that the C–N bonds in CIP were still remained. These ion chromatography results also proved an incomplete mineralization of CIP, which may generate various oxidized intermediates.

3.2. Degradation intermediates and generating mechanism

According to the published studies, three sites in CIP, including the C–F bond, the C=C bond in the quinolone moiety and the piperazine ring, can be attacked by the free radicals generated in the UV/ferrous-activated PS systems ([Ji et al., 2014; Mahdi-Ahmed and Chiron, 2014](#)). The screening of potential intermediates from the HRMS data was based on the possible transformations of these sites. Eventually, six steady intermediates were confirmed in the 280 nm UV/PS system. They were identified as $\text{C}_{15}\text{H}_{16}\text{FN}_3\text{O}_3$ (product A, m/z 306.1248), $\text{C}_{17}\text{H}_{18}\text{FN}_3\text{O}_4$ (product B, m/z 348.1354), $\text{C}_{15}\text{H}_{18}\text{FN}_3\text{O}_3$ (product C, m/z 308.1405), $\text{C}_{17}\text{H}_{16}\text{FN}_3\text{O}_3$ (product D, m/z 330.1248), $\text{C}_{17}\text{H}_{19}\text{N}_3\text{O}_4$ (product E, m/z 330.1448) and $\text{C}_{17}\text{H}_{16}\text{FN}_3\text{O}_4$

(product F, m/z 346.1198) (**Scheme 1**). The observed MS^2 spectra and related information of these products are presented in Figs. S3–S8 and Table S5.

Product A (**Fig. S3**) had a MW of 305.1176 Da, which was reported to be formed through the cleavage of C_2H_2 from the piperazinyl moiety (Pi et al., 2014b). Product B (**Fig. S4**) had a MW of 347.1281 Da. It was reported that product B may have a hydroxyl substitution at Site 10 of CIP (Mahdi-Ahmed and Chiron, 2014). The further oxidation of product B on the $C=C$ bond of quinolone moiety may form product C (**Fig. S5**), which had a MW of 307.1332 Da. Product D (**Fig. S6**) and product F (**Fig. S8**) may be the oxidized products on the piperazine ring of CIP, and the product E (**Fig. S7**) may have a hydroxyl substitution at side 5 on the $C-F$ bond. These results indicated that UV/PS oxidation mainly induced transformations of the peripheral moieties. In the previous study (Ou et al., 2016), only products A, B and E were observed in the 280 nm UV-only system, suggesting that products C, D and F were the characteristic intermediates in UV/PS oxidation of CIP.

The relative intensity variations and abundance variations of these intermediates are presented in **Fig. 2**. The dominating intermediates were product A and product B. The intensity of product A increased to approximate 1.2×10^6 at 10 min and then showed a decreasing tendency. Furthermore, the intensity of product B showed a slower increasing tendency with a maximum of 2.4×10^5 at 20 min. Undoubtedly, the hydroxyl addition at Site 10

and the breakage of piperazine ring were the dominant transformations in terms of the relative intensity in 280 nm UV/PS treatment. The four other intermediates were the minor products. Among them, product C increased to 4.5×10^4 at 30 min, and maintained at 3.2×10^4 within 60 min. Products D and E both had maximum values at 5 min. The intensity of product F increased to 2.2×10^4 at 30 min and disappeared at 60 min. These results also confirmed the proposed generative pathways from product B to product C, and from product D to product F. Of note, all these products were also observed in the 280 nm UV-LED/ H_2O_2 system; however, the abundance distribution was different (Ou et al., 2016). In the UV-LED/ H_2O_2 system, the dominating product was product B, while product A was the minor one, which may be attributed to the different reaction mechanisms between 280 nm UV/ H_2O_2 and UV/PS. In the UV/ H_2O_2 system, $OH\cdot$ oxidation was the main reaction. In the UV/PS system, the selective electron-transfer reaction of SO_4^{2-} was dominating, which generated $OH\cdot$ and other oxidizing agents (Neta et al., 1977). Therefore, the degradation of CIP may be a complex process, which included the reactions between CIP and $OH\cdot$, SO_4^{2-} , etc.

3.3. Proteome analysis

To reveal the safety of degrading intermediates, the proteomic analysis of *E. coli*, which involved biomarkers, protein expression

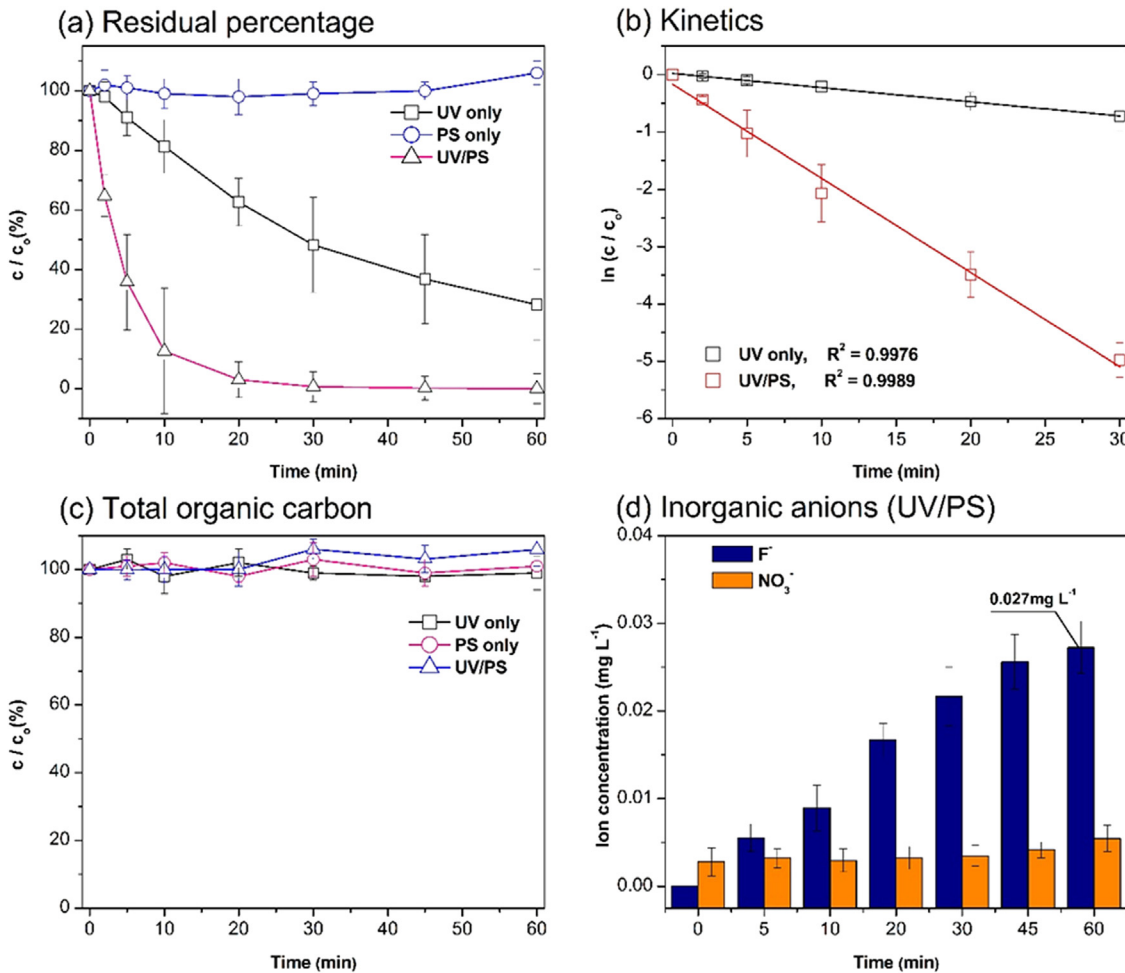


Fig. 1. Basic degradation efficiency of ciprofloxacin. Experimental conditions: solution temperature 25 ± 2 °C, pH 6.8–7.2, $[ciprofloxacin]_0 = 3 \mu M$, $[S_2O_8^{2-}]_0 = 210 \mu M$ (in PS-only and UV/PS experiments). All the experiments were carried out in triplicate with error bars representing the standard error of the mean.

and cellular metabolism networks, was investigated. Among 1102 quantifiable identified proteins, 56 and 110 proteins had significant up-regulated expression and down-regulated expression, respectively, in the *E. coli* exposed to 30 min UV/PS degrading CIP compared to untreated CIP (both $[CIP]_0 = 3 \mu\text{M}$, Table S7). The functional categories of these proteins in Panther database were annotated to verify their biological functions. In the molecular functions, 22 up-regulated expression proteins (Fig. 3a and Fig. S9a), including GapA and SodC, were hydrolase, isomerase, lyase, oxidoreductase and transferase those participated in catalysis. GapA is a glycolytic enzyme converting glyceraldehyde-3-phosphate to 1,3-bisphosphoglycerate for energy generation (Sangolgi et al., 2016). This housekeeping protein is essential for the maintenance of basic cellular functions and the upward expression in healthy situations (Liu et al., 2015). SodC is important for eliminating hydrogen peroxide and superoxide anion (Ribeiro et al., 2015). Therefore, their enhanced abundance indicated the improvement of cellular metabolism in *E. coli* exposed to degrading CIP.

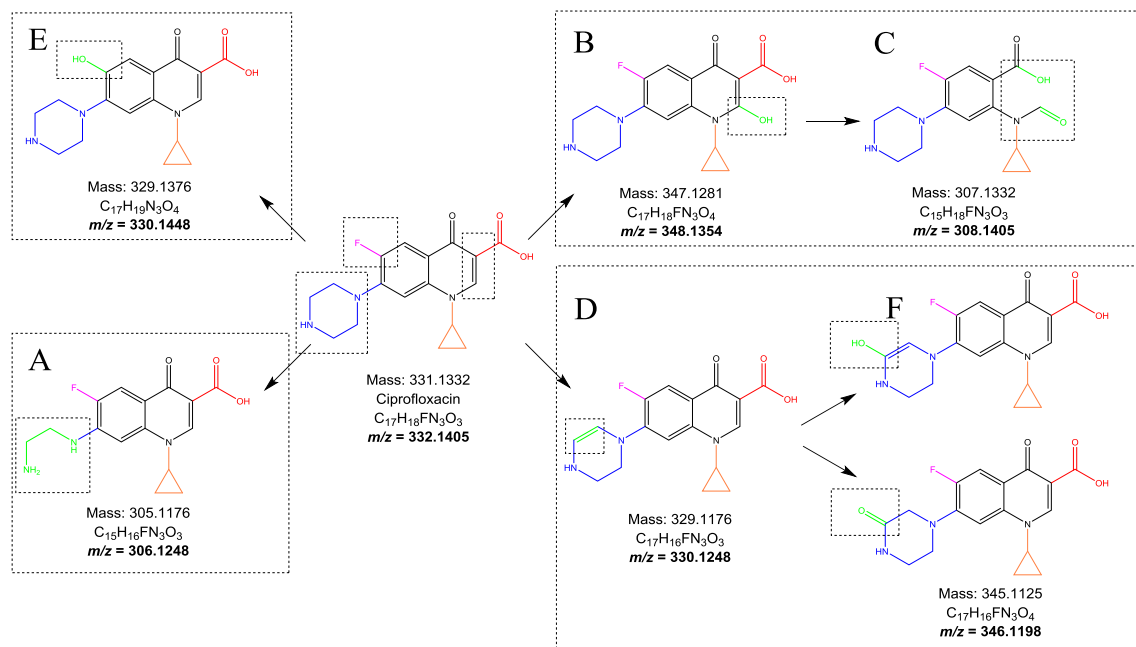
Except for some proteins with unknown functions, the other 16 up-regulated expression proteins were related to antioxidation, transport, binding, molecular structure and translation regulator activity (Fig. 3a). Five of them, including PstS, YadG, ArtP, AtpC and DppD, were associated with substrate transport. Furthermore, PstS, YadG, ArtP and DppD are the ATP-binding cassette (ABC) transporters responsible for transporting various substrates across membranes (Yang and Driessens, 2015). KEGG Motif search identified that YadG, ArtP and DppD had 13 (Fig. S10a), 13 (Fig. S10b) and 8 (Fig. S10c) motifs, respectively. Since both ATPases associated with diverse cellular activities (AAA) domain and ABC domain were related to substrate binding (Zhang et al., 2016), the up-regulated synthesis of these transporters with various substrate binding domains suggested that the substrate transport and metabolism of *E. coli* exposed to degrading CIP were significantly improved.

Compared to the up-regulated proteins, some down-regulated proteins were also acted as deaminase and ligase that participated in catalysis (Fig. 3a and Fig. S9a). Riboflavin biosynthesis protein RibD was a deaminase, acting as the central component of

the cofactors flavin mononucleotide and flavin adenine diucleotide, which were the ligand of pyruvate dehydrogenase and succinate dehydrogenase (Gudipati et al., 2014). None significantly differentiated synthesis of pyruvate dehydrogenase E1 component and NAD(P)H-flavin reductase indicated that the decreased formation of RibD did not trigger the decline of riboflavin production. The down-regulated ligases included valine-tRNA ligase ValS and serine-tRNA ligase SerS, which catalyzed the attachment of valine and serine to tRNA. They played important roles in DNA translation and protein formation (Iwawaki and Tokuda, 2011). Their decreased formation was one of the reasons why the synthesis of some proteins those regulated by ValS and SerS significantly reduced in the current study.

When classified the protein functions based on the biological processes, the categories of the up-regulated proteins were metabolic process, localization, cell communication, biological regulation and stimulus response (Fig. 3b). The metabolic process was mainly related to primary metabolic process, phosphate/nitrogen-containing compound metabolic process, biosynthetic process, catalytic process, vitamin metabolic process, precursor metabolites and energy generation (Fig. S9b). This finding inferred that the toxicity of the degrading products of CIP was significantly decreased because most of the up-regulated proteins were associated with the primary metabolic process rather than the responses to stress and toxic substance. Although the decreased expression proteins also exhibited similar biological processes, the detailed pathways they involved were different (Fig. 3b and Fig. S9b).

To confirm this inference, the interactions in biological networks among proteins were investigated through String analysis (string-db.org) at high confidence. No up-regulated synthesis proteins enriched in some networks (Fig. S11), whereas, several interactions among partial down-regulated proteins were found (Fig. 4). Seventeen down-regulated proteins, especially the key node proteins Lon, Hfq, Tig, Obg, SecA and SecF, were enriched in the first network that mainly involved: (1) the export of protein across the cell membrane, (2) the control of stress response, cell cycle and ribosome biogenesis, (3) the degradation of abnormal proteins and RNA expressed under stresses, (4) the regulation of mRNA



Scheme 1. Proposed generative pathways for the ciprofloxacin intermediates after 280 nm UV/PS treatment.

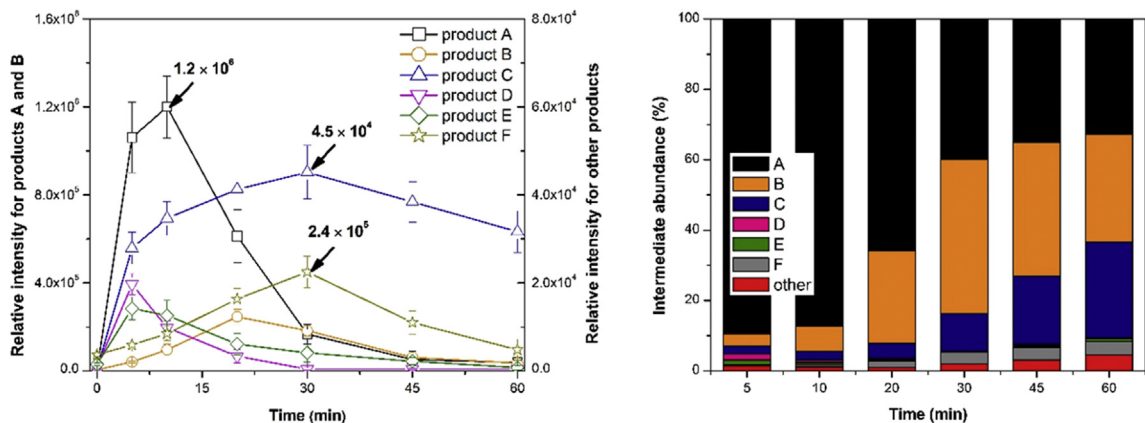


Fig. 2. Relative intensity and abundance variations of observed intermediates after 280 nm UV/PS treatment. The relative intensity indicates the peak area of extract ion chromatogram from MS/MS data, which has a dimensionless unit.

translation in response to envelope stress. The decreasing expression of these proteins in response to toxic stresses confirmed that the abnormal expression of proteins and RNA obviously reduced, indicating the toxicity of UV/PS degrading CIP was significantly lower than that of intact CIP.

The second network, containing proteins Tmk, ThyA, Fold, FolA, PurK, Amn, PurB and DeoD, was primarily associated with purine and pyrimidine metabolism, decreasing the transformation of

adenine, hypoxanthin, adenosine 5'-monophosphate, deoxyadenosine, deoxyguanosine (Fig. S12) and deoxythymidine 5'-phosphate (Fig. S13). Therefore, the low expression of these proteins illustrated that it was unnecessary for cells to generate more energy to maintain cellular metabolism under the exposure to UV/PS treated CIP. The third network (NarG, NuoA, NuoC and DmsB) was also related to the decreasing energy metabolism, which further confirmed the above results. Both respiratory nitrate reductase 1 alpha chain (NarG) and dimethyl sulfoxide reductase chain B (DmsB) serve as reductases under anaerobic condition, catalyzing nitrate to nitrite, and dimethyl sulfoxide to dimethyl sulfide (Bouchal et al., 2010; Gonzalez et al., 2013), respectively. The down regulation of the proteins in this network indicated a decreasing energy metabolism of cells exposed to UV/PS degrading products both in aerobic and anaerobic conditions.

3.4. Antibacterial activity

E. coli was used as the reference organism for the estimation of the residual antibacterial activity. The variation of antibacterial activity of the treated CIP solution was determined qualitatively by measuring the inhibition halo diameter. The typical results are presented in Fig. 5, where the diameter of inhibition halo decreased from 21 mm (control) to 9 mm (10 min), and finally disappeared after 20-min reaction, suggesting a total elimination of antibacterial activity. Similar antibacterial activity reduction of incomplete degrading antibiotic was reported in the studies using quantitative assessments (Dodd et al., 2009; Cai and Hu, 2016). Since no mineralization was observed (Fig. 1c), the elimination of antibacterial activity was attributed to the transformation of CIP.

CIP is supposed to interact with two targets, DNA gyrase and topoisomerase IV, resulting in DNA replication failure. The quinolone backbone is the basic framework, while the peripheral moieties play different roles in antibacterial activity. According to the HRMS results, products A and B were the primary intermediates. The piperazine ring can directly interact with DNA gyrase or topoisomerase IV (Ma et al., 1999), thus, the fracture of it (product A) may have significant suppression on the antibacterial activity. Since Site 10 at CIP is very close to the site for DNA gyrase (or topoisomerase IV) binding, the addition of a hydroxyl to this site (product B) can also inhibit the antibacterial activity (Domagala, 1994). Furthermore, the carboxyl group is important for cleaving or perturbing DNA (Tillotson, 1996). The consecutive oxidation of product B to form product C resulted in damage of carboxyl group, which had a significant inhibition of antibacterial activity. However,

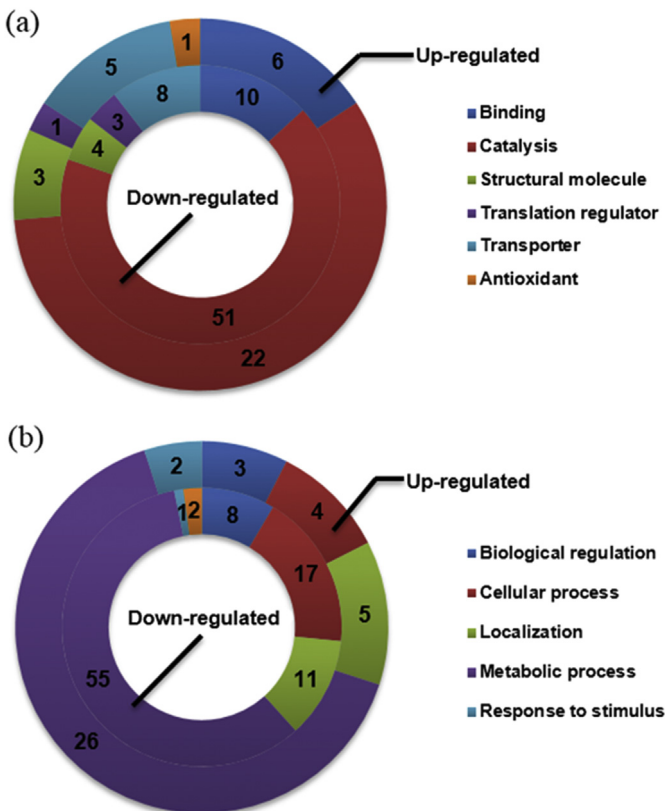


Fig. 3. Function categories of differently expressed proteins in *Escherichia coli* after exposure to 30 min UV/PS degrading ciprofloxacin compared to untreated ciprofloxacin. Experimental conditions: solution temperature 25 ± 2 °C, pH 6.8–7.2, $[ciprofloxacin]_0 = 3 \mu\text{M}$, $[S_2O_8^{2-}]_0 = 210 \mu\text{M}$. (a) Molecular function of up-and down-regulated synthesis proteins, (b) Biological function of up-and down-regulated synthesis proteins.

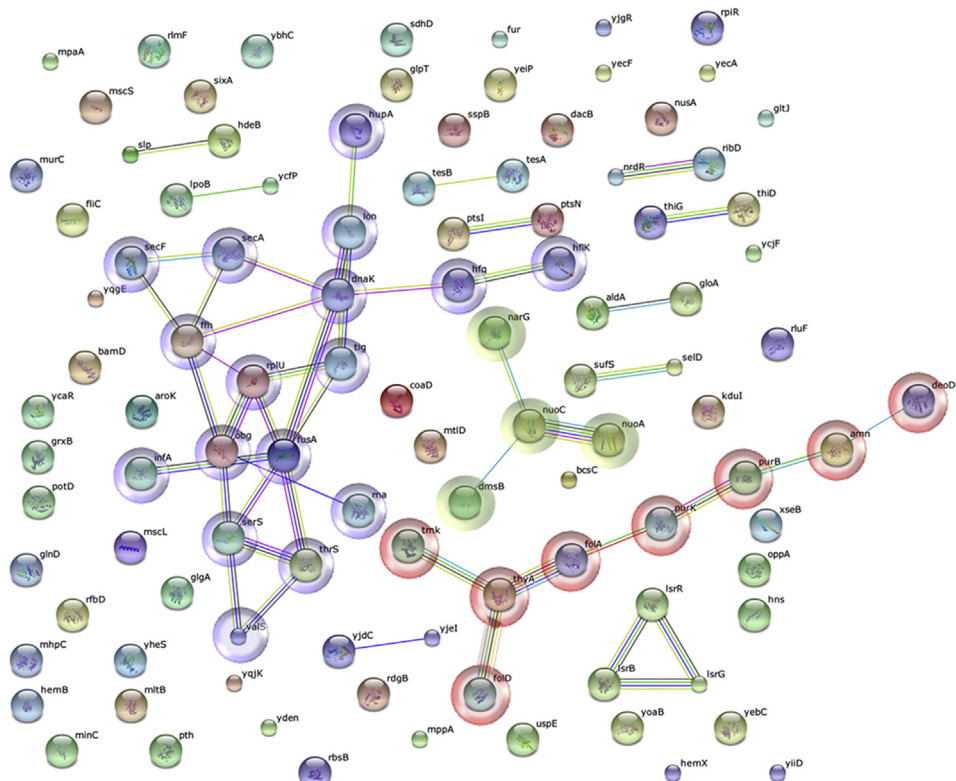


Fig. 4. Biological networks of down-regulated synthesis proteins in *Escherichia coli* exposed to UV/PS degrading ciprofloxacin compared to untreated ciprofloxacin.

in comparison with CIP, the exposure of *E. coli* to UV/PS degrading products did not trigger the significantly differentiated expression of DNA gyrase subunit A and B, DNA topoisomerase 1 and DNA topoisomerase 4 subunit A in the current study, which is not consistent with these earlier findings. CIP exhibited inhibitive effect on 110 significant down-regulated expression proteins (Table S7), suggesting that DNA gyrase and topoisomerase IV may not be the most sensitive targets. The influence of CIP on proteins not just limited in the scope of some target molecules but a whole protein network and various metabolism pathways.

3.5. Cost evaluation

The results of the UV-LED/PS treatment in terms of the removal efficiency and antibacterial activity reduction were observed to be rather good. However, its energy and material cost still need to be evaluated. The electrical energy per order (EE/O) value was used. The EE/O is defined as the electrical energy in kilowatt per hours (kWh) required to degrade a specific contaminant by one order of magnitude in 1 m³ contaminated water or air. Generally, EE/O can be calculated using Eq. (6).

$$\text{EE/O} = \frac{Pt}{60V} \quad (7)$$

where P is the total electrical power used for the treatment (kW); t is the irradiation time (h); and V is the volume of treated water (m^3). Detailed procedure of the calculation method was reported in Ref. (He et al., 2013). The electrical energy cost values (EE/O_e) were calculated to be 0.01155 and 0.00086 kWh m^{-3} order $^{-1}$, respectively, for the 280 nm UV-LED-only and UV-LED/PS ($[\text{S}_2\text{O}_8^{2-}] = 210 \mu\text{M}$) treatment (Table S6). For UV-LED/PS treatment using different dosage PS, the chemical oxidant cost values (EE/O_c , the cost of PS) increased from 0.0043 to 0.0867 kWh m^{-3} order $^{-1}$ when $[\text{S}_2\text{O}_8^{2-}]$ increased from 42 to 840 μM .

The EE/O value was calculated by taking into account the EE/O_e and the EE/O_c. Thus, it can be used to represent the overall cost and to guild the optimization. Obviously, the addition of PS consumed a large proportion of cost in total EE/O. The EE/O_c consumed 84.7% and 96.4% in the UV-LED/PS treatment using 84 and 210 μM PS, respectively. And this ratio continuously increased when PS dosage increased. Of note, the total EE/O of UV-LED/PS treatment using 84 μM was 0.01038 kWh m⁻³ order⁻¹, which was lower than the total EE/O of UV-LED only treatment. However, the EE/O of UV-LED/

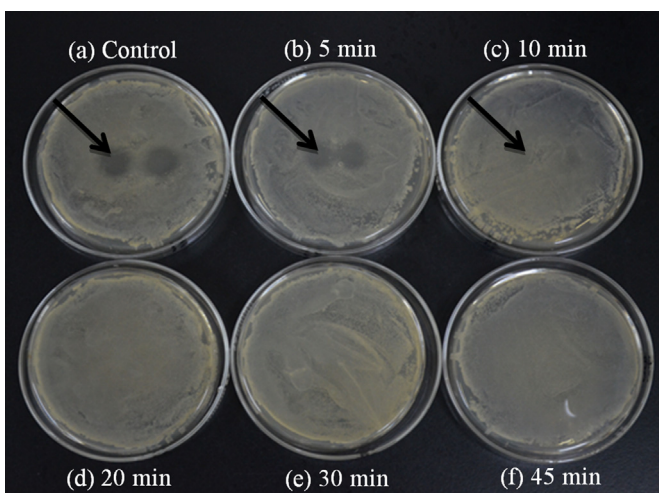


Fig. 5. *Escherichia coli* inhibition halo at different times of 280 nm UV/PS treatment. Initial *Escherichia coli* dosage = 1.2×10^8 cfu mL $^{-1}$.

PS treatment using 210 μM was 0.02253 kWh m⁻³ order⁻¹. These results indicated that the overall cost of UV-LED/PS treatment can be adjusted by changing the addition dosage of PS. Compared with UV-LED/H₂O₂ treatment (0.00643 kWh m⁻³ order⁻¹, [CIP]₀ = 30 μM, [H₂O₂]₀ = 300 μM) (Ou et al., 2016), the EE/O values of UV-LED/PS treatment was higher. However, the EE/O values obtained were significantly lower than the values in the experiments using conventional mercury lamps (Tan et al., 2013).

4. Conclusion

To conclude, the 280 nm UV/PS treatment induced a moderate degradation of CIP, which had a high transformation efficiency and a low mineralization. The HRMS data demonstrated that the primary intermediates included C₁₅H₁₆FN₃O₃ and C₁₇H₁₈FN₃O₄. The transformation pathway involved the cleavage at piperazine ring, the addition of the hydroxyl and the further oxidation on quinolone backbone. The iTRAQ proteomic assessment identified a total of 56 and 110 proteins with significant up- and down-regulation, respectively, in the *E. coli* exposed to UV/PS degraded CIP compared to untreated CIP. Most of the up-regulated proteins were associated with primary metabolic processes rather than response to stress and toxic substance, confirming that the toxicity of the degradation intermediates was significantly decreased. The current study provides insights into the action mechanisms of CIP and its degrading products on *E. coli*, clarifying that the UV/PS moderate degradation is an alternative cost-effective and safety treatment strategy for quinolones.

Acknowledgments

This project was supported by the National Natural Science Foundation of China (Grant Nos. 51308224, 21577049), the Science and Technology Planning Project of Guangdong Province, China (Grant No. 2014A020216014).

Appendix A. Supplementary data

Supplementary data related to this article can be found at <http://dx.doi.org/10.1016/j.chemosphere.2016.09.031>.

References

- An, T., Yang, H., Li, G., Song, W., Cooper, W.J., Nie, X., 2010. Kinetics and mechanism of advanced oxidation processes (AOPs) in degradation of ciprofloxacin in water. *Appl. Catal. B Environ.* 94, 288–294.
- Avetta, P., Pensato, A., Minella, M., Malandrino, M., Maurino, V., Minero, C., Hanna, K., Vione, D., 2014. Activation of persulfate by irradiated magnetite: implications for the degradation of phenol under heterogeneous photo-Fenton-like conditions. *Environ. Sci. Technol.* 49, 1043–1050.
- Bouchal, P., Struhárová, I., Budinská, E., Šedo, O., Vyhlídalová, T., Zdráhal, Z., van Spanning, R., Kučera, I., 2010. Unraveling an FNR based regulatory circuit in *Paracoccus denitrificans* using a proteomics-based approach. *Bba-Protein. Protom* 1804, 1350–1358.
- Brienza, M., Ahmed, M.M., Escande, A., Plantard, G., Scrano, L., Chiron, S., Bufo, S., Goetz, V., 2016. Use of solar advanced oxidation processes for wastewater treatment: follow-up on degradation products, acute toxicity, genotoxicity and estrogenicity. *Chemosphere* 148, 473–480.
- Cai, Q., Hu, J., 2016. Decomposition of sulfamethoxazole and trimethoprim by continuous UVA/LED/TiO₂ photocatalysis: decomposition pathways, residual antibacterial activity and toxicity. *J. Hazard. Mater.* <http://dx.doi.org/10.1016/j.jhazmat.2016.06.006> (in press).
- Dodd, M.C., Kohler, H.-P.E., Von Gunten, U., 2009. Oxidation of antibacterial compounds by ozone and hydroxyl radical: elimination of biological activity during aqueous ozonation processes. *Environ. Sci. Technol.* 43, 2498–2504.
- Domagala, J.M., 1994. Structure-activity and structure-side-effect relationships for the quinolone antibiotics. *J. Antimicrob. Chemother.* 33, 685–706.
- Doorslaer, X.V., Demeestere, K., Heynderickx, P.M., Caussyn, M., Langenhove, H.V., Devlieghere, F., An, V., Dewulf, J., 2013. Heterogeneous photocatalysis of moxifloxacin: identification of degradation products and determination of residual antibacterial activity. *Appl. Catal. B Environ.* 138, 333–341.
- Gonzalez, P.J., Rivas, M.G., Mota, C.S., Brondino, C.D., Moura, I., Moura, J.J., 2013. Periplasmic nitrate reductases and formate dehydrogenases: biological control of the chemical properties of Mo and W for fine tuning of reactivity, substrate specificity and metabolic role. *Coord. Chem. Rev.* 257, 315–331.
- Gudipati, V., Koch, K., Lienhart, W.-D., Macheroux, P., 2014. The flavoproteome of the yeast *Saccharomyces cerevisiae*. *Bba-Protein. Proteom* 1844, 535–544.
- He, X., Armah, A., Dionysiou, D.D., 2013. Destruction of cyanobacterial toxin cylindrospermopsin by hydroxyl radicals and sulfate radicals using UV-254nm activation of hydrogen peroxide, persulfate and peroxyxonosulfate. *J. Photochem. Photobiol. A* 251, 160–166.
- Iwawaki, T., Tokuda, M., 2011. Function of yeast and amphioxus tRNA ligase in IRE1alpha-dependent XBP1 mRNA splicing. *Biochem. Biophys. Res. Commun.* 413, 527–531.
- Ji, Y., Ferronato, C., Salvador, A., Yang, X., Chovelon, J.-M., 2014. Degradation of ciprofloxacin and sulfamethoxazole by ferrous-activated persulfate: implications for remediation of groundwater contaminated by antibiotics. *Sci. Total. Environ.* 472, 800–808.
- Kjeldal, H., Zhou, N.A., Wissenbach, D., von Bergen, M., Gough, H.L., Nielsen, J., 2015. Genomic, proteomic and metabolite characterization of gemfibrozil-degrading organism *Bacillus* sp. GeD10. *Environ. Sci. Technol.* 50, 744–755.
- Lapara, T.M., Burch, T.R., McNamara, P.J., Tan, D.T., Mi, Y., Eichmiller, J.J., 2011. Tertiary-treated municipal wastewater is a significant point source of antibiotic resistance genes into Duluth-Superior Harbor. *Environ. Sci. Technol.* 45, 9543–9549.
- Liu, C., Nanaboina, V., Korshin, G.V., Jiang, W., 2012. Spectroscopic study of degradation products of ciprofloxacin, norfloxacin and lomefloxacin formed in ozonated wastewater. *Water Res.* 46, 5235–5246.
- Liu, S., Zhu, P., Zhang, L., Li, Z., Lv, Q., Zheng, S., Wang, Y., Lu, F., 2015. Increased glyceraldehyde-3-phosphate dehydrogenase expression indicates higher survival rates in male patients with hepatitis B virus-associated hepatocellular carcinoma and cirrhosis. *Exp. Ther. Med.* 9, 1597–1604.
- Liu, Y., Chen, S., Zhang, J., Gao, B., 2016. Growth, microcystin-production and proteomic responses of *Microcystis aeruginosa* under long-term exposure to amoxicillin. *Water Res.* 93, 141–152.
- Ludmilla, A., Anastasios, M., Garrison, S., 2010. Inhibition of photosynthesis by a fluoroquinolone antibiotic. *Environ. Sci. Technol.* 44, 1444–1450.
- Ma, Z., Chu, D.T., Cooper, C.S., Li, Q., Fung, A.K., Wang, S., Shen, L.L., Flamm, R.K., Nilius, A.M., Alder, J.D., 1999. Synthesis and antimicrobial activity of 4H-4-oxoquinolizine derivatives: consequences of structural modification at the C-8 position. *J. Med. Chem.* 42, 4202–4213.
- Mahdi-Ahmed, M., Chiron, S., 2014. Ciprofloxacin oxidation by UV-C activated peroxyxonosulfate in wastewater. *J. Hazard. Mater.* 265, 41–46.
- Min, L., Wei, D., Zhao, H., Du, Y., 2014. Genotoxicity of quinolones: substituents contribution and transformation products QSAR evaluation using 2D and 3D models. *Chemosphere* 95, 220–226.
- Neta, P., Madhavan, V., Zemel, H., Fessenden, R.W., 1977. Rate constants and mechanism of reaction of sulfate radical anion with aromatic compounds. *J. Am. Chem. Soc.* 99, 163–164.
- Oberlé, K., Capdeville, M.J., Berthe, T., Budzinski, H., Petit, F., 2012. Evidence for a complex relationship between antibiotics and antibiotic-resistant *Escherichia coli*: from medical center patients to a receiving environment. *Environ. Sci. Technol.* 46, 1859–1868.
- Ou, H.-s., Ye, J.-s., Ma, S., Wei, C.-h., Gao, N.-y., He, J.-z., 2016. Degradation of ciprofloxacin by UV and UV/H₂O₂ via multiple-wavelength ultraviolet light-emitting diodes: effectiveness, intermediates and antibacterial activity. *Chem. Eng. J.* 289, 391–401.
- Paul, T., Dodd, M.C., Strathmann, T.J., 2010. Photolytic and photocatalytic decomposition of aqueous ciprofloxacin: transformation products and residual antibacterial activity. *Water Res.* 44, 3121–3132.
- Pi, Y., Feng, J., Song, M., Sun, J., 2014a. Degradation potential of ofloxacin and its resulting transformation products during Fenton oxidation process. *Chin. Sci. Bull.* 59, 2618–2624.
- Pi, Y., Feng, J., Sun, J., Song, M., Sun, J., 2014b. Oxidation of ofloxacin by Oxone/Co²⁺: identification of reaction products and pathways. *Environ. Sci. Pollut. R.* 21, 3031–3040.
- Qinqin, Z., Ai, J., Yi, W., Hong, L., Kunping, W., Hui, P., Zhaomin, D., Jianying, H., 2014. Occurrences of three classes of antibiotics in a natural river basin: association with antibiotic-resistant *Escherichia coli*. *Environ. Sci. Technol.* 48, 14317–14325.
- Ribeiro, T.P., Fernandes, C., Melo, K.V., Ferreira, S.S., Lessa, J.A., Franco, R.W., Schenck, G., Pereira, M.D., Horn, A., 2015. Iron, copper, and manganese complexes with *in vitro* superoxide dismutase and/or catalase activities that keep *Saccharomyces cerevisiae* cells alive under severe oxidative stress. *Free. Radic. Biol. Med.* 80, 67–76.
- Rodrigues-Silva, C., Maniero, M.G., Rath, S., Guimarães, J.R., 2013. Degradation of flumequine by the Fenton and photo-Fenton processes: evaluation of residual antimicrobial activity. *Sci. Total. Environ.* 445, 337–346.
- Sangolgi, P.B., Balaji, C., Dutta, S., Jindal, N., Jarori, G.K., 2016. Cloning, expression, purification and characterization of *Plasmodium* spp. glyceraldehyde-3-phosphate dehydrogenase. *Protein Expre. Purif.* 117, 17–25.
- Tan, C., Gao, N., Deng, Y., Zhang, Y., Sui, M., Deng, J., Zhou, S., 2013. Degradation of antipyrene by UV, UV/H₂O₂ and UV/PS. *J. Hazard. Mater.* 260, 1008–1016.
- Tillotson, G.S., 1996. Quinolones: structure-activity relationships and future predictions. *J. Med. Microbiol.* 44, 320–324.
- Yang, N., Driessens, A.J., 2015. The *saci_2123* gene of the hyperthermoacidophile

- Sulfolobus acidocaldarius* encodes an ATP-binding cassette multidrug transporter. *Extremophiles* 19, 101–108.
- Zhang, Y., Li, Y., Zhang, Y., Wang, Z., Zhao, M., Su, N., Zhang, T., Chen, L., Wei, W., Luo, J., 2016. Quantitative proteomics reveals membrane protein-mediated hypersaline sensitivity and adaptation in halophilic *Nocardiopsis xinjiangensis*. *J. Proteome Res.* 15, 68–85.
- Zhou, L., Ying, G., Liu, S., Zhao, J., Yang, B., Chen, Z., Lai, H., 2013. Occurrence and fate of eleven classes of antibiotics in two typical wastewater treatment plants in South China. *Sci. Total. Environ.* 452–453, 365–376. C.